THE ELASTO-PLASTIC TRANSITION IN MAGNESIUM ALLOYS

K. Vanna Yang, C.H. Cáceres[*]
ARC Centre of Excellence for Design in Light Metals, Materials Engineering
School of Engineering, The University of Queensland, Brisbane, QL, 4072, Australia
C.N. Tomé
MST Division Los Alamos National Laboratory Los Alamos NM 87545 USA

Keywords: AZ31 alloy; Magnesium; Elasto-plastic transition; Kocks-Mecking analysis; Strain hardening; Twinning; Prism slip

Abstract

Published neutron diffraction data on internal strains in a textured polycrystal of AZ31 alloy and tensile data for a random polycrystal of Mg are discussed from two complementary points of view, a purely phenomenological and a formal crystallographic one. It is suggested that the transition to full plasticity involves two different fractions of the grains population, at different strains. The role of texture and twinning are discussed. Critical experiments to test some of the hypotheses on how the elasto-plastic transition develops are proposed.

Introduction

The present paper is the result of an exchange of ideas between the US and Australia based authors concerning the meaning of the elasto-plastic transition in textured AZ31 alloy, and by extension, Mg and its alloys in general. It aims at identifying weak points in the understanding of the phenomenon as well as to advance a few hypotheses. Kocks-Mecking analysis of published data is used as a framework to the discussion.

The onset of gross plastic deformation in randomly oriented Mg and Mg alloys involves a microplasticity stage which may extend to nearly 1 % strain in which basal slip, and sometimes twinning, are active, followed by a linear hardening stage during which general plasticity develops [1, 2]. The linear hardening stage may extend to strains as large as 10 % or even higher, depending on the grain size.

In a recent neutron diffraction study by Agnew et al. [3] on textured AZ31 alloy, the linear hardening stage past the first ~2 % and up to nearly 10 % strain was described as a protracted elasto-plastic (e/p) transition, akin to what is observed in composite materials in which the apparent, or macroscopic, strain hardening rate reflects the load-sharing between soft- and hard-oriented grains in the polycrystalline aggregate.

This interpretation of the linear hardening stage is at odds with recent analyses of the strain hardening behaviour of texture-free pure Mg polycrystals [4, 5] which show, based on the Kocks-Mecking method of analysis, that athermal accumulation of forest dislocations should determine the strain hardening rate of polycrystalline Mg in much the same way as in FCC metals at low temperature or with a low value of the stacking fault energy, hence with a strong tendency to planar glide, accounting for the observed linear hardening in the first ~10 % strain.

[*] Corresponding author, c.caceres@uq.edu.au, Fax:+ 61-7-33467015, Phone: +61-7-33654377.

In the next sections the Kocks-Mecking phenomenological method of analysis [6] is applied to the lattice strain data collected by Agnew et al. [3] in tensile specimens of cold rolled alloy AZ31, and subsequently compared with a similar analysis made on the tensile flow curve of a texture-free polycrystal of pure Mg to assess the rate at which the increase of internal stresses in soft- and hard-oriented grains relates to the macroscopic strain hardening rate as the materials are deformed.

Data for Analysis

The macroscopic flow curve and the internal strain-applied stress curves obtained by the in-situ strain measurements of the alloy are reproduced in Figures 1 and 2. Figure 1 also includes the tensile flow curve of a fine grained (grain size 19 μm [7]) pure Mg polycrystal.
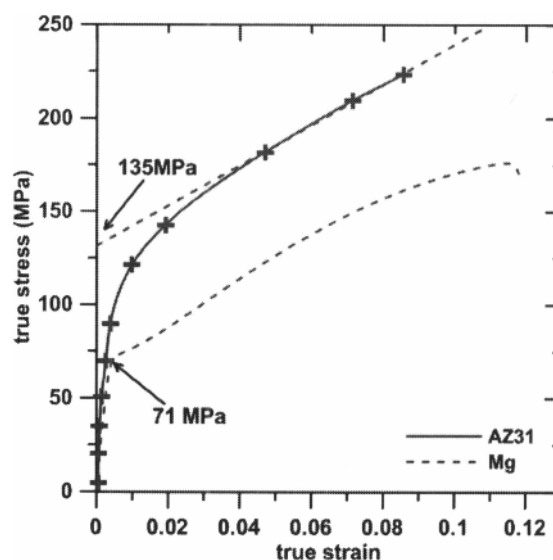

Figure 1 The solid line is the stress-strain curve for in-plane tension of alloy AZ31, reproduced from Figure 1-a of reference [3]. In this and the following figures the symbols (crosses in this case) denote the loci of the in-situ neutron diffraction measurements. The dashed line is the tensile flow curve of a Mg polycrystal reproduced from references [4, 7]. The yield strength of both materials is indicated by arrows (see text).

The flow curves of Figure 3 were obtained by converting the internal (lattice) strains of Figure 2 to internal stresses through Hooke's law (Equation 1). Only the elastic strains parallel to the tensile axis are considered in the analysis.

$$\sigma_i = E(hk.l) * \varepsilon_i \qquad (1)$$

where σ_i is the internal stress, $E(hk.l)$ is the Young's modulus normal to the relevant crystallographic planes (hk.l), and ε_i is the lattice strain along the same direction. The values for $E(hk.l)$ listed in Table 1 were calculated using standard formulae and the compliance constants from Table 2, all taken from [8-10]. Equation 1, for simplicity, assumes unconstrained uniaxial loading.

Table 1 Young's modulus in the direction perpendicular to the $(hk.l)$ crystallographic planes, calculated as described in [8]

plane	(10.0)	(10.1)	(10.3)
E_{hkl} (GPa)	45.45	43.29	45.03

Table 2 Compliance constants for pure Mg [9, 10]

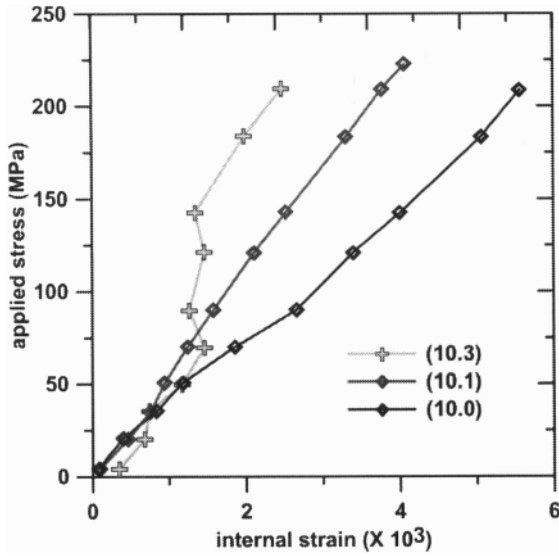| Compliance constants (10^{-11} Pa)				crystallographic parameter (nm)	
s_{11}	s_{33}	s_{44}	s_{13}	a	c
2.20	1.97	6.10	0.50	0.318	0.5131

Figure 2 Internal strain and applied stress for grains with normal to their prismatic and pyramidal planes parallel to the stress axis of the AZ31 specimen of Figure 1. In this and remaining figures (hk.l) identifies the crystallographic planes of which the normals are parallel to the stress axis.

In Figure 3-a, the internal stress in all three grain orientations increases almost identically up to ~25 MPa, diverging for larger applied stresses. The (10.3) normal direction parallel to the stress axis shows a relatively short microplasticity regime followed by a plateau, ascribed in the original reference to twinning, and a linear hardening regime at larger strains. The (10.1) and (10.0) normal directions exhibit a longer microplasticity regime and linear hardening past ~2 % strain, without any major perturbation from twinning. The strain hardening rates at large strains are similar, i.e., the stress-strain curves of Figure 3-a are nearly parallel to

each other. In Figure 3-b the flow curves are back extrapolated to determine the respective yield strengths σ^* for the analysis of the next section. The yield strengths of the macroscopic curves are indicated in Figure 1.
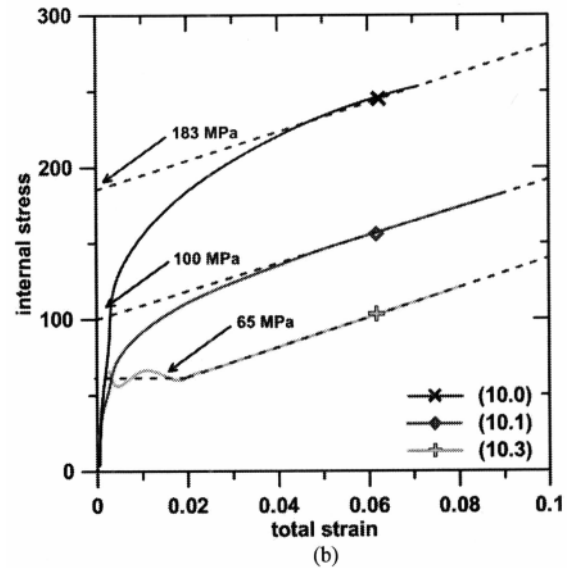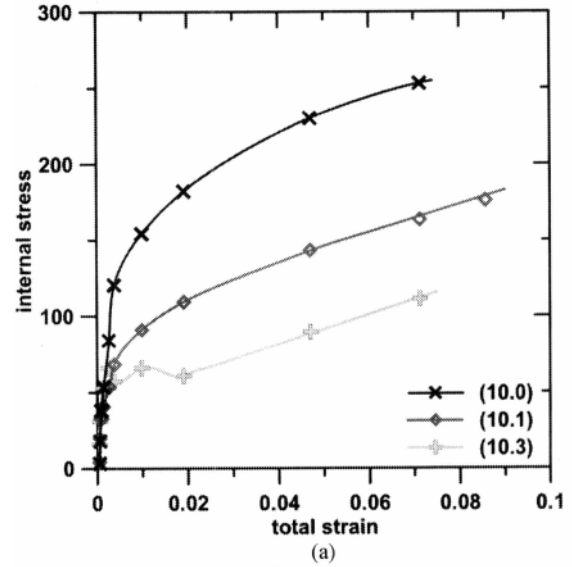

(a)

(b)

Figure 3 (a) Internal stress-total strain curves calculated using Equation 1 for the curves of Figure 2; (b) Determination of the offset stresses, σ^*, by back extrapolation of the large strain flow curves of Figure 3-a.

Kocks-Mecking analysis The formalism was applied to the present materials as described in detail in references [4, 11] for pure Mg polycrystals, according to:

$$(\sigma - \sigma^*)\frac{d\sigma}{d\varepsilon} = (\sigma - \sigma^*)\Theta_h = (\sigma - \sigma^*)\frac{E}{C} \qquad (2)$$

128

where σ is the flow stress, ε is the true strain and $\Theta_h = \frac{d\sigma}{d\varepsilon} = E/C$ is the strain hardening rate when hardening is controlled by athermal accumulation of dislocations, σ^* is the offset stress determined for the alloy in Figures 1 and 3-b as suggested by Kocks and Mecking [12] by back-extrapolation (dashed lines), and C is a constant whose value depends on the Taylor factor M. With $M = 4.5$ [5] and $E = 44$ GPa, $\Theta_h \approx E/32 = 1.4$ GPa, a value closely matched by random polycrystals of Mg [4, 11].

The graphical version of Equation 2, called "$\Theta\sigma$-plot", is shown in Figures 4-a and 4-b for the curves of Figures 1 and 3, respectively; the initial slopes of the respective $\Theta\sigma$ plots are in the range of 1.0 GPa to 2.0 GPa, matching the expected value of 1.4 GPa quite closely.

Discussion

Flow behavior A number of differences and some crucial similarities between the flow curves of Figure 1 are relevant to the present analysis. The onset of the microplasticity stage (i.e., the departure from pure elastic behavior) occurs at fairly low stresses (25-50 MPa) for both materials. For the pure Mg macroscopic flow begins at 71 MPa with an incipient plateau, most likely connected to twinning, and a subsequent linear hardening stage that extends to 8-10 % strain. The alloy, in contrast, exhibits a round shape from about 75 MPa and up to ~2 % strain, suggesting the a gradual development of internal stresses. At large strains the flow curves of both materials become parallel to each other. At about 10% strain the pure Mg flow stress tends to saturate; a similar behavior is hinted by the alloy, although the data available do not go far enough. Further details of the yielding process are discussed below.

Kocks-Mecking behavior Under an athermal regime of dislocations accumulation [4, 5], the $\Theta\sigma$-plot of a plastically deforming Mg polycrystal starts with a straight line through the origin of gradient $\Theta_h = 1.4$ GPa. This behavior is shown in Figure 4-a, curve labeled Mg. The initial gradients of the corresponding $\Theta\sigma$-plots for the macroscopic and the internal stresses of the alloy (figures 4-a and b) closely match that of the pure Mg. Therefore it may be asserted that the elastic loading of the hard-oriented grains in the alloy is largely determined by the monotonic accumulation of dislocations in the plastic grains past the first 2 % strain, mimicking what occurs in the pure Mg polycrystal.

An overall picture of how the plasticity evolves in the either one of the materials past the purely elastic regime can be construed as follows, partly following the descriptions given in [4, 5]. Prior to the onset of microyielding, internal (elastic) strain develops linearly in all grains, differing only by the elastic anisotropy, which in Mg is minor. When basal slip is activated in the grains with the most favorable orientation to the stress axis, the microplasticity stage starts. During this stage soft-oriented grains diminish their share of elastic strain and hard-oriented grains compensate by becoming more highly stressed. The overall hardening rate at this stage is therefore determined by the load shedding between the (micro) plastic and elastic grains. The end of the microplasticity stage is determined by the activation of the first available hard slip system, which experiments show is prism slip [13]. This seems to enable sufficient polyslip in the plastically active grains, marking the onset of macroplasticity; the strain

hardening rate consequently drops to a value that commensurate with athermal accumulation of dislocations, (1.4 GPa, Figure 4).
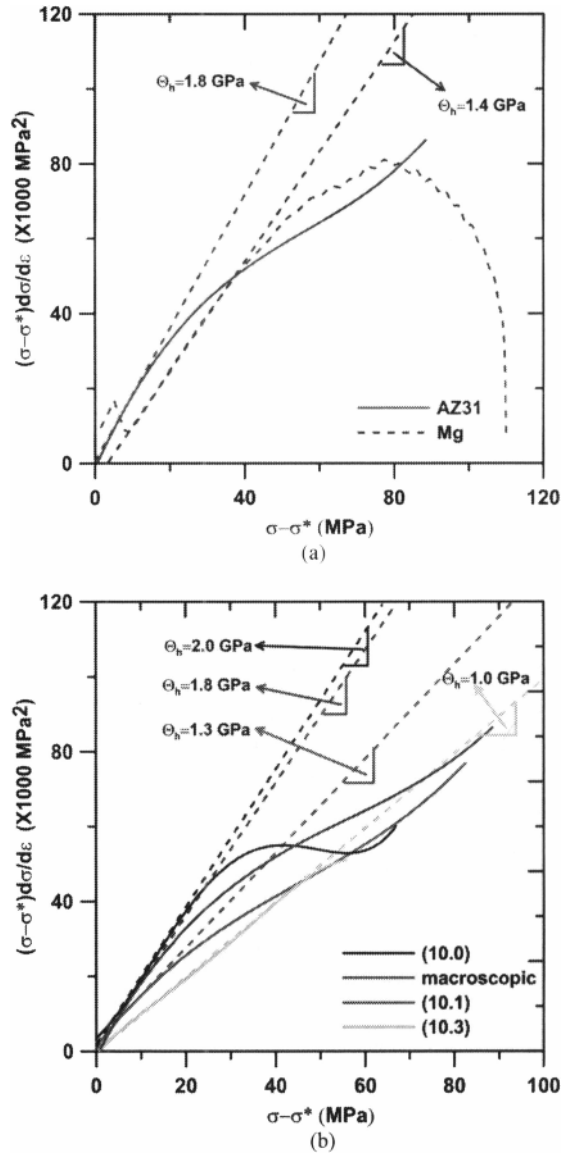

(a)

(b)

Figure 4 $\Theta\sigma$-plots for the (a) AZ31 and pure Mg flow curves of Figure 1 and (b) internal stresses curves of Figure 2. The straight dashed lines are lines of best fit to the low stress region of the respective $\Theta\sigma$-plots, with the slope as indicated. The curve labeled 'macroscopic' in 4-b corresponds to the flow curve of alloy AZ31 in Figure 4-a and Figure 1.

The differences in behavior at yield between the alloy and the pure Mg made evident by Figure 1 can be accounted for as follows: in the random polycrystal there are enough soft-oriented grains to ensure that any hard-oriented grains are rapidly wrapped out by fully plastic grains, and the transition from the microplasticity stage to fully plasticity is very short, as shown by Figure 1.

For the alloy, the rounded flow curve in the first 2 % strain is an indication that the fraction of soft-oriented grains is initially not enough to wrap around the hard-oriented ones. As the stress increases, the fraction of plastic grains increases monotonically until they are enough to wrap around the remaining elastic grains. Pat this point, the strain hardening rate is determined by the forest hardening of the plastic grains and the e/p transition is over. Twinning plays an important part in the pure Mg as shown by the incipient plateau in Figure 1 and although the neutron diffraction data indicates limited activity, it seems likely that the combination of slip and twinning is sufficient to mock true polyslip [14] in the alloy as well, and thus avoid the need for 5 independent slip systems in both materials leading to the observed linear hardening.

It is of interest to note in passing that the behaviour of the AZ31 alloy specimen is remarkably consistent with that of polycrystalline CoTi as described by Wollmershauser et al. [15]. Due to the plastic anisotropy of the intermetallic, and similarly to Mg, the soft slip system <100>{011} is activated first, creating a steep microplasticity stage, followed by an extended linear hardening stage which extend to strains as large as ~20 %. The transition between the micro and the macro plasticity stages, which replicates the behavior of Mg, is triggered by the activation of the <111>{1-10} hard slip system.

Yield surface and full plasticity From a more formal point of view, it may be argued that the "end of the e/p transition" should meet the von Mises-Taylor criterion for full plasticity, which is only possible when the stress "lodges" in a vertex of the yield surface and stops "sliding" along it (at least for a substantial amount of strain) [16]. The concept is of course well established for FCC metals since a vertex provides the 5 independent slip systems required. For the AZ31 alloy specimen the neutron diffraction results showed that no slip systems are active up to ~25 MPa, only basal slip is active between 25 and 75 MPa, at a strain of about 0.5 %, then basal and prism systems are active between 75 and 175 MPa and the onset of pyramidal slips is identified past 175 MPa, at strains above 4~5 %. Since, in principle, basal and prism slips are insufficient to accommodate full plasticity, the internal stress will not reach a vertex until pyramidal slip is fully activated in a significant fraction of crystals, delaying the onset of full plasticity to strains approaching 10 %. This description of course ignores the enabling role of twinning discussed earlier.

Returning to the phenomenological approach, Mecking et al.'s suggested that the yield surface of plastically anisotropic materials becomes increasingly isotropic at large strains. The behaviour of the present materials closely conforms to this assertion since, on the one hand, the macroscopic flow curves become parallel to each other past the strain of 2 %; and on the other, at $\Theta_h = 1.4$ GPa, the strain hardening behaviour of both materials, and in particular that of the alloy's internal stresses, is consistent with athermal forest hardening and independent of the initial texture.

The role of texture It is possible to produce a rather simplistic but unified description of the e/p transition for both the alloy and the pure metal considering that there are two e/p transitions, independent of each other, affecting different fractions of the grain population, and occurring at different strains in the flow curve.

The first e/p transition follows the description given in the preceding section. Figure 1 shows that in the Mg specimen this transition takes place at well-defined values of the stress (~71 MPa in Fig. 1) and strain, whereas in the alloy it extends over the first ~2 % strain, leading to the rounded flow curve. In both materials it is followed by a linear hardening stage.

Past ~5 % strain the internal stresses are high enough to activate pyramidal slip in the (still elastic) hardest oriented grains, and true von Mises-Taylor plasticity begins to take place in those grains, gradually propagating to other hard-oriented grains. This in practice constitutes a second e/p transition affecting both the pure Mg and the alloy alike. The second transition develops gradually as it is driven by the athermal forest hardening of the soft-oriented grains. The strain hardening rate decreases slowly during the process, which is completed at ~10 % strain, when the flow stress saturates.

The first transition may be termed "global", whereas the second could be considered "latent" or "alien".

With reference to the curves of Figure 1, the effect of crystallographic texture can now be understood as follows: in the random polycrystal of Mg the proportion of soft-oriented grains is large enough to ensure a rapid and well defined global transition. By contrast, the scarcity of soft-oriented grains leads to an extended "Masing-solid" behavior on the side of the alloy [17], giving raise to the rounded shape of the flow curve. The increasing difference in flow stress level between the alloy and the pure Mg is consistent with internal stresses developing as in dispersion hardened materials [18, 19].

Figure 1 also shows that the linear hardening stage is quite extended in the pure Mg, and this is due to the sharpness of the global transition. For the alloy, texture extends the global transition up to the onset of the latent one, shortening the linear hardening regime. In a sense, it may be asserted that in the presence of a strong texture the global and latent e/p transitions overlap, effectively extending the overall yielding process over a strain of ~ 10 %.

Limitations to the approach Despite the generally self-consistent picture produced by the Kocks-Mecking analysis, and largely due its phenomenological nature, the description given above suffers from several shortcomings and limitations, as detailed below.

The use of Equation 1 to create the "internal flow curves" of Figure 3, albeit very convenient, is somewhat misleading as the strain used in the x-axis is coming from a subset of grains which may not be even close neighbors. The "crystallographic stiffness" is therefore not the directional Young's modulus of the single crystal, because none of the contributing crystals in the subset experiences the same elastic stress state. (As a matter of fact, the crystallographic stiffness is different for different textures.) However, since Mg's elastic tensor is close to isotropic, any absolute errors in Figure 3 cannot be too large, and it should be kept in mind that the curves of Figure 3 are only used to determine the internal strain hardening rate, thus the conclusions extracted from Figure 4-b are quite likely realistic .

The strain rate for athermal forest hardening was obtained using a value of $M = 4.5$ for the Taylor factor. Such value was obtained as a relation between strain hardening rates (following Mecking et

130

al.'s [20] approach), and as such it represents only a lower bound when it comes to stresses, making the "expected" value for $\Theta_h = 1.4$ GPa a lower bound to the strain hardening rate by forest hardening.

The above treatment of twining ignores a most important difference between the alloy and the pure metal. It is known that solid solution hardening delays the onset of twinning, and the effect is anisotropic, i.e., it affects the soft and hard slip systems in opposite directions and with different strengths [21, 22]. This difference is made evident in Figure 1 by the significant activity of twinning at low strains in the pure Mg flow curve. In the alloy, only the (10.3) system exhibits limited effects of twinning (Figure 3a).

A further oversimplification relates to the assumption that soft grains physically wrap hard grains, the latter assumed to remain elastic as hard inclusions would in a dispersion hardened material. A similar elasto-plastic behaviour would result from the activation of twinning in a subset of grains and basal slip in others, followed by prismatic slip in still other subset. This alternative conception dispenses with the need to preserve a subset of grains completely elastic, and implies that the strain interval over which some grains remain purely elastic is small.

Likewise, there is no need for the stresses to be on a vertex of the yield surface in every grain for the aggregate to be fully plastic. Simulations show that depending on relative CRSSs and texture 3 or 4 average active systems per grain usually suffice to accommodate deformation (see for instance Figures 8b, 8c and 11b in [10]). In other words, individual grains need not to follow the macro strain tensor, provided their average behavior does. This blurs somewhat the boundary between the global and latent e/p transitions. For instance, the description given above assumes that at 5% strain pyramidal slip gets activated in grains which are still fully elastic, while in practice many of those grains may have basal or prism slip activated already.

Further experiments and modelling Experiments that should enable separating the elastic and the plastic components of the strain could involve Bauschinger effect type of tension-compression test, and measuring the x-ray peak broadening. The former would enable quantifying the amount of elastic recovery at any given strain whereas the second would allow assessing the dislocation density evolution. With these data a more detailed EPSC simulation would be possible, incorporating the overall enabling role of twinning, the anisotropy of solid solution hardening and the effect of texture.

Conclusions

The Kocks-Mecking analysis was applied to the macroscopic and the internal stress-total strain curves of grain populations with different orientations in AZ31 sheet metal with a strong basal texture, and compared with the tensile behavior of a randomly oriented fine grained Mg polycrystal.
Strain hardening rates of 1~2 GPa were obtained for the internal stresses in all three crystallographic directions as well as for the macroscopic flow curve of the alloy. These values match that of the pure Mg polycrystal (1.4 GPa) and appear consistent with athermal accumulation of forest dislocations.

There is a first, or global, elasto-plastic transition involving basal, prism slip and twinning, leading to a linear strain hardening stage due to athermal forest hardening.

The activation of pyramidal slip in the hardest-oriented elastic grains triggers a second, or latent, e/p transition at a strain of ~5 % in both materials. This transition develops slowly with the strain, driven by the forest hardening of the soft-oriented grains. The whole process is completed at a strain of ~10%.

The presence of crystallographic texture in the alloy extends the global transition over a strain of ~2 %, in contrast with the random polycrystal of Mg, for which it occurs at a very well defined point in the flow curve.

References

[1] A. Akhtar, E. Teghtsoonian, Metall. Trans. A, 2 (1971) 2757-2763.
[2] A. Blake, C.H. Cáceres, in: N.R. Neelameggham, H.I. Kaplan, B.R. Powell (Ed.) *Magnesium Technology 2005*, The Minerals, Metals and Materials Society (TMS), Warrendale, PA, 2005, pp. 403-407.
[3] S.R. Agnew, C.N. Tomé, D.W. Brown, T.M. Holden, S.C. Vogel, Scripta Mater., 48 (2003) 1003-1008.
[4] C.H. Cáceres, A.H. Blake, Mater. Sci. Eng. A, 462 (2007) 193-196, http://dx.doi.org/10.1016/j.msea.2005.12.113.
[5] C.H. Cáceres, P. Lukác, Philos. Mag. A, 88, http://dx.doi.org/10.1080/14786430801968611 (2008) 977-989,
[6] U.F. Kocks, H. Mecking, Prog. Mater. Sci., 48 (2003) 171-273.
[7] C.H. Cáceres, G.E. Mann, J.R. Griffiths, Metall. Mater. Trans. A, 42 (2011) 1950-1959, DOI: 10.1007/s11661-010-0599-2.
[8] J.M. Zhang, Y. Zhang, K.W. Xu, V. Ji, Thin Solid Films, 515 (2007) 7020-7024, 10.1016/j.tsf.2007.01.045.
[9] H.B. Huntington, Sol. St. Physics, 7 (1958) 213-351.
[10] U.F. Kocks, C.N. Tomé, H.-R. Wenk, Texture and Anisotropy, Cambridge University Press, Cambridge, 1998.
[11] C.H. Cáceres, P. Lukác, A. Blake, Philos. Mag. A, 88 (2008) 991-1003, http://dx.doi.org/10.1080/14786430701881211.
[12] S. Sannes, H. Gjestland, H. Westengen, C. Dorum, O. Lohne, in: SAE 2005 World Congress & Exhibition, , , Detroit, MI, USA, 2004, pp. 725-731.
[13] A. Akhtar, E. Teghtsoonian, Materials Transactions (JIM), 9, supplement (1968) 692-697.
[14] U.F. Kocks, D.G. Westlake, Transactions AIME, 239 (1967) 1107-1109.
[15] J.A. Wollmershauser, C.J. Neil, S.R. Agnew, Metall. Mater. Trans. A, 41 (2010) 1217-1229, 10.1007/s11661-009-9990-2.
[16] C.N. Tomé, U.F. Kocks, Acta Metall., 33 (1985) 603-621,
[17] G. Masing, in: (Ed.) *Proc. 2nd Int. Congr. Applied Mechanics*, 1926, pp. 332-335.
[18] L.M. Brown, W.M. Stobbs, Philos. Mag., 23 (1971) 1185-1199.
[19] L.M. Brown, W.M. Stobbs, Philos. Mag., 23 (1971) 1201-1233.
[20] H. Mecking, U.F. Kocks, C. Hartig, Scripta Mater., 35 (1996) 465-471.
[21] D. Nagarajan, C.H. Caceres, J.R. Griffiths, Acta Polonica, In press (2012).
[22] A. Akhtar, E. Teghtsoonian, Acta Metall., 17 (1969) 1351-1356.